WILEY ONLINE LIBRARY
Early View publication on
www.wileyonlinelibrary.com
(issue and page numbers not yet assigned;
citable using Digital Object Identifier – **DOI**)

J. Biophotonics 1–8 (2013) / **DOI** 10.1002/jbio.201300067

Journal of
BIOPHOTONICS

FULL ARTICLE

Hyperspectral enhanced dark field microscopy for imaging blood cells

Giulia Sacco Verebes[**,1], *Michele Melchiorre*[**,2], *Adianez Garcia-Leis*[2,3], *Carla Ferreri*[2], *Carla Marzetti*[1], *and Armida Torreggiani*[*,2]

[1] Antigenia srl Unipersonale, Via Montebello 2, 40121 Bologna, Italy
[2] ISOF, Consiglio Nazionale delle Ricerche, Via P. Gobetti 101, 40129 Bologna, Italy
[3] Instituto de Estructura de la Materia, CSIC, Serrano, 121, 28006-Madrid, Spain

Received 2 May 2013, revised 12 June 2013, 12 July 2013, accepted 13 July 2013
Published online 6 August 2013

Key words: red blood cell, granulocytes, hyperspectral imaging, dark field microscopy

Supporting information for this article is available free of charge under http://dx.doi.org/10.1002/jbio.201300067

In this work, a novel methodology based on hyperspectral imagery with enhanced Darkfield microscopy for probing and characterizing changes in blood cell components was tested. Two main categories of blood cells were analyzed, red and white blood cells. Unique spectral signatures of ordinary and most common deformed morphologies of red blood cells were identified. Moreover, examination of white blood cells allowed to characterize and differentiate active from inactive cells.
The findings indicate the ability of this technique to detect changes in light scattering property of blood cells due to their morphological properties Since pathological states can alterate the discocyte shape, this preliminary, but promising application of the hyperspectral analysis to blood cells can be useful to evaluate significant correlations of blood cell spectral features in healthy and pathological conditions. The combination of the quali- and quantitative spectral signatures of hyperspectral imaging microscopy with the information of the subject health conditions may provide a new tool for clinical applications.

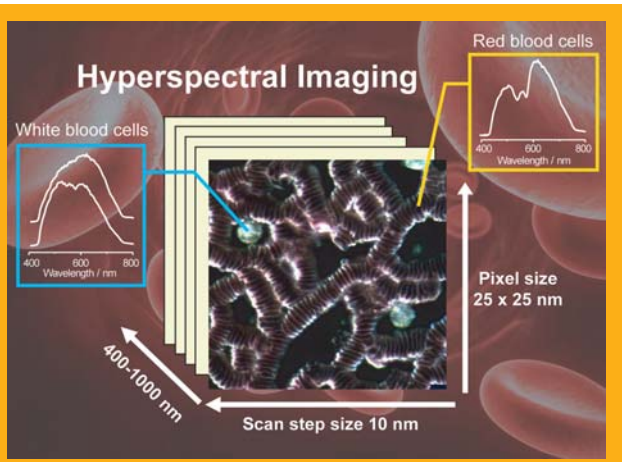

Hyperspectral imagery of red and white blood cells represented as a data cube.

1. Introduction

Due to its easy access and key roles in biological activity, analysis of human blood allow routine monitoring of many pathologies, as well as health levels in humans more generally. A large number of analytical techniques are employed for these purposes, among them optical analytical approaches for distin-

* Corresponding author: e-mail: armida.torreggiani@isof.cnr.it
** The authors contributed equally

guishing specific components in complex biological mixtures often offer advantages of speed, ease-of-use, and cost. Microscopic examination of blood samples is the widely used method for the detection of some parasites and for diseases diagnosis. Unfortunately, some cell structures, cell organelles and particularly bacteria and virus are commonly too small to be fully observed with an optical microscope. Therefore, an electron microscope is required but, at the same time, it is impossible to view living cells due to the sample preparation requiring that living cells be fixed, frozen and dehydrated. Furthermore, many processes can be seen occurring only in living cells, i.e. cellular interactions, diffusion, phagocytosis, cytoplasmic streaming, etc. To follow them a microscope with an optical system that allows the observation of live cells at high resolution and contrast without an invasive sample preparation process is necessary.

Hyperspectral Imaging System (HIS) is a rapidly growing modality for biomedical applications [1–3]. The technique provides both spectral and spatial information in one measurement and does not require contact between the object and the sensor. The HIS integrated-darkfield-based microscope technology is specifically designed to give quantitative mapping of surfaces and for material identification, and used i.e. for nanomaterials and functional groups added to them [4–5]. In the biological field, it starts to show potentials for spectral characterization of bacteria and pathogens in the blood and mapping them in tissue and other environments [6–7]. It is interesting that no special fluorescent markers are required, however an exhaustive library of spectral data is still needed in order to provide adequate references for the analysis.

Here we demonstrate the effectiveness of an hyperspectral enhanced dark-field microscope (EDFM), consisting of an enhanced dark-field illumination system attached to a standard light microscope, for probing and characterizing changes in blood cell components, potentially connected with health levels. Thanks to no need of sample preparation and use of a low power light source, producing low heating and, as consequence a reduced phototoxicity, this system can provide a view of live cell and cell processes while they are occurring [8].

Under enhanced Darkfield conditions, blood cells appears brighter than in other methods due to Koehler and main features of Critical illumination by collimated light source at oblique angles, thus obviating the need for staining agent or a contrast agent to visualise more details in samples [9]. In addition, the HIS spectrometer allows analysis of scattered light at pixel-by pixel level, thus samples can be imaged by acquiring hundreds of contiguous wavelengths or bands producing extensive spatial and spectral data for each pixel [10].

Since pathological condition affecting red blood cells (RBCs) can lead to significant alterations to the discocyte shape, advanced new tools have been developed in the past two decades to quantify the mechanical properties of live biological cells [11]. For example, atomic force microscope (AFM), optical (laser) tweezers, microfluidic devices, and tomographic phase microscopy (TPM) have been increasingly used to quantify and characterize different mechanobiological signatures of human RBCs [12–14].

Scattering from blood cells has attracted the interest of many researchers in the area of biomedical science, since it is connected to the morphological properties of cells and to pathological states involving the modification of them [15–17]. In fact, alterations such as the erythrocyte morphology reflect chemical variances or physical abnormalities of red blood cell (RBC) membrane itself or of its content. For example, the light scattering properties of RBCs have been found to be affected by adenosine 5′-triphosphate (ATP)-driven membrane metabolic remodeling, since RBC membrane loses its biconcave shape in the absence of ATP and undergoes the morphological transformation to echinocyte [18, 19]. Progressive alteration of the scattering signal has been evidenced also in the development of malaria-inducing parasites and it can distinguish the specific diseases states [20, 21]. Recently, scattering spectroscopy in conjunction with cross-polarization imaging has been used for laboratory malaria research, facilitating point-of-care diagnosis [22]. In addition, light scattering of RBCs is widely used in flow cytometry for measuring size and hemoglobin concentration distribution [23] and scattering problems involving a single RBC or multiple RBCs have been also investigated by employing various numerical methods, such as Mie-series approximations [24, 25], surface integral equation, etc. [26, 27].

In this paper we report an investigation of hyperspectral microscopic analysis of blood cells with the aim at showing that it is possible to build-up a library of spectral data characteristics of the different morphologies of blood cells. In particular, the ability of this hyperspectral imagery technique was tested on two main categories of blood cells: red and white blood cells (RBCs and WBCs, respectively). Ordinary and most common deformed morphologies of RBC were analyzed discovering the specificity of spectral features connected to 3 deformed shapes, namely stacked erythrocytes (rouleaux formation), echinocytes, and irregularly shaped RBCs. We anticipate that the identification of unique spectral patterns allowed to follow-up the development of surface changes, which might be useful to understand better the correlation of morphological features with the cellular environment and health conditions. Moreover, examination of WBCs (granulocytes) allowed to characterize and differentiate active from inactive cells.

2. Experimental

2.1 Sample preparation

Blood specimens were given by a clinical laboratory for routine analysis and used in experiments. A total of 27 samples were obtained from both healthy individuals and individuals having non-allergic food hypersensitivity (5 samples). Our aim was to individuate spectral signatures associable to the most common morphological alterations of blood cells, therefore a strict correlation with health conditions is out of the scope of this work. The samples from individuals having non-allergic food hypersensitivity were chosen as examples to test the effectiveness to built up spectral libraries.

The blood was collected in Ethylenediaminetetraacetic acid (EDTA) anticoagulant and stored at 4 °C for no more than 24 h, checking that in this period no changes occurred to the spectral features. The blood samples (10 μL) were placed on glass slides and sandwiched with cover glasses. No need of sample fixing process was required.

2.2 Enhanced dark-filed microscopy and hyperspectral imaging

RBCs and WBCs were examined in air and at room temperature by using an enhanced dark field illumination system (CytoViva, Auburn, AL) attached to an Olympus microscope (EDFM). The system consisted of a CytoViva 150 dark field condenser in place of the microscope original condenser, attached *via* a fiber optic light guide to a Solarc 24 W metal halide light source (Welch Allyn, Skaneateles Falls, NY). The CytoViva dark field method picks up forward scatter from the sample at angles greater than 20 degrees from the forward light propagation, over a scattering cone of approximately 100 degrees. The angle of the forward incident light is approximately 70 degrees off of the normal to the sample slide, so as to miss the aperture of the objective lens. The scattering is isotropic in the plane of the sample slide. The angle is such that the direct illumination does not enter the objective lens, rendering a dark field. Therefore the sensitivity of this angular configuration is high, since the scatter is superimposed on a dark background.

Improved optical performances are obtained by pre-aligned Koehler and main feature of Critical illumination. Koehler illumination is pre-aligned in the device by fixing the light source precisely on the entrance slit of the condenser. This allows the user to adjust a focus point on the sample, which is a useful feature of Critical illumination, and is achieved when the condenser is aligned with the objective to find the focal point on the sample. Thus, Koehler illumination is initially fixed, and then CytoViva can be adjusted (up or down) to find the proper position and size of an illuminated spot for Critical illumination.

Scattering intensity strongly depends upon the light wavelength, thus corrections for image distortions are indispensable to achieve the highest possible resolution. The objective lenses used in the CytoViva microscope are color-corrected over visible wavelengths and in particular over the 450–650 nm range where hemoglobin absorption produces a spectral signature. The other components of the system, including microscope and spectrograph, are similarly corrected. Moreover, any chromatic aberration from the condenser is constant since the illumination path and angles of light are prealigned.

A 100× oil objective with an iris (Olympus UPlanAPO fluorite, N.A. 1.35–0.55) was integral to the system. CytoViva optical illumination system uses a cardioid annular condenser that ensures a large angle of illumination. In this configuration, the sample is illuminated by a hollow cone of parallel rays. The light penetrating the sample and the coverslip enters the oil immersion objective far from the optical axis. This set-up improves resolution and offers a strong contrast for unstained samples that are barely visible in regular transmitted light microscopy [28].

Measurements were performed without sample manipulation in order to avoid artifacts.

Spectral data within each pixel of the scanned field of view were captured with a CytoViva spectrophotometer and integrated charged-coupled device (CCD) camera. The spectrophotometer operates in 400–1000 nm range (VNIR). The spectral resolution was 2.5 nm and pixel size was 25 nm.

In the display images a linear intensity scale without enhancement of the contrast has been used (linear 2%). Since multi-colour images are shown, a colour scale bar, indicating intensity scale along with it, was included in each image.

Spectral data were analysed by using the CytoViva Hyperspectral analysis software program (ENVI 4.4 and ITT Visual Information Solutions). Hyperspectral imagery is typically collected (and represented) as a data cube with spatial information collected in the X–Y plane, and spectral information represented in the Z-direction. Image processing and analysis involved some steps that are necessary for building the spectral libraries (spectral endmembers), such as the ones shown as example for stacked RBCs and granulocytes in Figure S1 (see Supplementary Information). The spectral endmembers were obtained by the selection of a region of interest (ROI) on the scanned sample. The ROI selection allows to choose pixels that best represent the morphological state of blood cells (or functional state as

in the case of WBCs). The hyperspectral images of RBCs with a regular biconcave shape (discocyte) served as the guide for choosing the endmembers associated with the ordinary morphology of RBCs (healthy state).

When the characteristic spectral endmembers were identified, they were saved into a spectral library by the ENVI software for the subsequent spectral mapping of the hyperspectral images of other samples. Each spectra included in the library was sampled from a single pixel imaged with a 100× objective. Finally, a classical mapping method, namely, Spectral Angle Mapper (SAM), was employed to measure the similarity between the image pixels and the endmember pixels. SAM implements by calculating the angle between the image and endmember spectra, treating them as vectors in n-D space where, n represents the number of bands. The best match was achieved when the angle between endmember and sample spectra was the least.

The libraries were mapped onto images of interest by false-colouring a pixel if they were within 0.1 radians of one of the spectra in the library.

Its class distribution reveals the information about the relative contribution from each of the endmembers in the image scenes. This method is insensitive to illumination since the SAM algorithm uses only the vector direction and not the vector length.

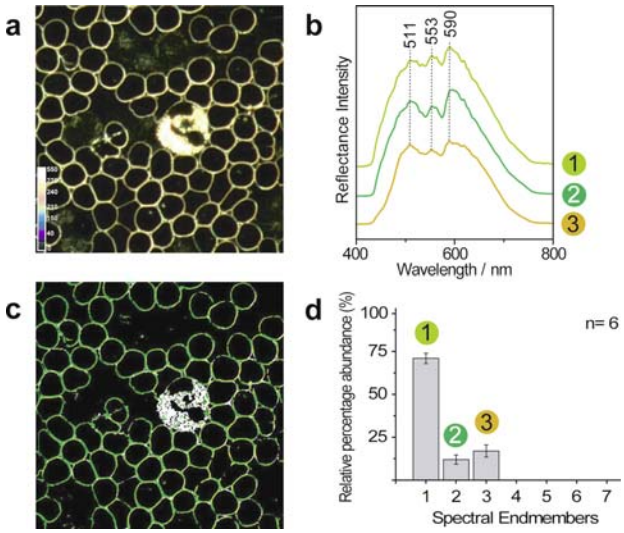

Figure 1 Ordinary RBCs having regular biconcave shape (discocyte). (**a**) Hyperspectral image, (**b**) Spectral signatures in the 400–800 nm, and (**c**) Map of the spectral endmembers in the hyperspectral image of the sample obtained by SAM analysis (colored areas indicate the matching with the spectral profiles); (**d**) Histogram reporting the relative percentage abundance of the spectral patterns in the maps of hyperspectral images of six blood samples (n standing for the number of the analysed samples). Images were acquired by using 100× objective. The intensity values are color-coded according to the color scale bar. All images are 60 μm × 60 μm.

3. Results and discussion

3.1 Red Blood Cells (RBCs)

A series of initial measurements was performed to evaluate the ability of the Hyperspectral imagery analysis to differentiate the RBC morphology. The biconcave shape of RBC is essential feature of its biological function and from a biochemical standpoint it could be explained as an effect due to the interplay of lipid bilayer membrane with cytoskeletal proteins. Comparative proteomic and lipidomic of RBC membrane in health and disease have recently shown a good potential in shedding light on RBC differences between health and disease, leading potentially to the identification of markers and to a better understanding of disease mechanisms [29–32]. Aside from its discocyte shape, erythrocytes may take on alternate shapes, and some anomalies have just been connected to pathological conditions [11, 33]. Healthy RBCs, appearing to be round, evenly shaped and freely floating, were characterized (Figure 1a).

Light scattering from ordinary RBCs gave rise to three VNIR spectra, all characterized by the presence of three peaks at about 510, 555 and 590 nm, among them the latter had a slightly higher intensity (Figure 1b). The effectiveness of the matching tool was proved by using these spectral endmembers in the image scenes of samples from healthy individuals (as example see Figure 1c). The SAM classification images showed the distribution of all the ordinary RBCs endmembers in the images and the quantification of their relative abundance. Among the three spectra, one (Endmembers 1) represents the main contribution to the total scattering of RBCs (∼70%), whereas that from the other two, which are less relevant, is almost similar (∼15%) (Figure 1d). Of consequence, spectral pattern 1 can be considered the most representative for RBCs in ordinary state (Figure S2 in Supplementary Information).

Another class of deformed RBCs is represented by the stacked erythrocytes (Figure 2a). These refer to erythrocytes that stick together, yielding an appearance similar to a stack of coins (rouleaux). The formation of these aggregates can be a natural phenomenon induced by biological factors, i.e. due to blood plasma proteins and under sufficiently low flow rates; rouleaux are easily decomposed to their individual cell constituent as blood flow increases, as happen in healthy individuals [34]. Due to this aggregation process, the scattering properties of RBCs significantly change, as evidenced previously by the-

oretical calculations [27]. Light scattering of stacked erythrocytes gave mainly rise to two spectral signatures (Figure 2b), systematically associable to different regions of the RBC rouleaux: one from the roleaux outline, and another one from the inner part of the surface. The first was just found for ordinary RBCs (Endmember 2) and the second is peculiar of this RBCs state (Endmember 4). The latter is characterized by three peaks, among them one significantly increased in intensity and shifted towards the red region (from ~590 to ~620 nm). By performing the spectral mapping of some samples (as example Figure 2c), this spectral pattern was found to be the most representative of roleaux-shaped RBCs (~90%) (Figure 2d).

It's worth to pointing out that the periodic roughness on the surface of the roleaux along the direction of symmetry, due to aggregated RBCs, causes a large variety in local curvatures of cell membrane, and of consequence, light scattering gives rise to many other spectra (Figure S3 in Supplementary Information). Among them, Endmember 4 resulted to be the most representative of this morphological state since the mapping of it onto several images from different samples systematically gave rise to very good match.

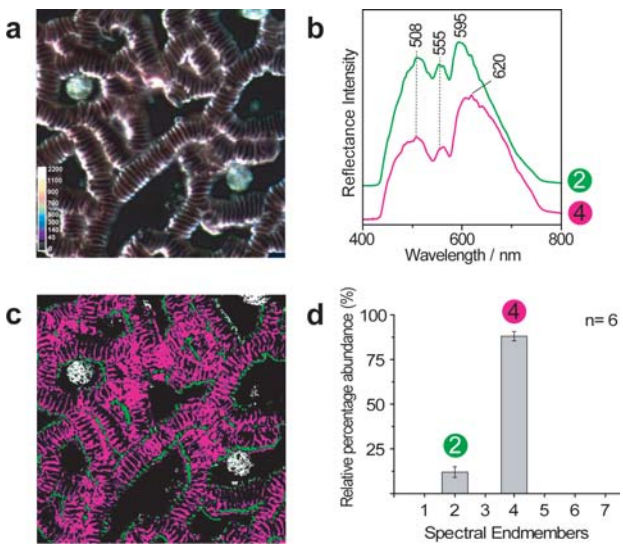

Figure 2 Stacked RBCs forming roleaux. (**a**) Hyperspectral image, (**b**) Spectral signatures in the 400–800 nm, and (**c**) Map of the endmembers in the hyperspectral image of the sample (colored areas indicate the matching with the spectral profiles); (**d**) Histogram reporting the relative percentage abundance of the spectral patterns in the maps of hyperspectral images of six blood samples (*n* standing for the number of the analysed samples). Images were acquired by using 100× objective. The intensity values are color-coded according to the color scale bar All images are 60 μm × 60 μm.

The existence of a spectral library associable to this aggregation state can be important in order to give quantitative information in case of unhealthy conditions. In fact, rouleaux formation can be also symptomatic of an underlying disease or condition. For examples, in some pathological cases the capillarity circulation is seriously affected because nonseparable rouleaux are formed, as well as cerebrovascular accidents, acute myocardial infractions and diabetes are closely related to excessive RCB aggregation [35, 36].

Other two types of RBCs with an alterate morphology were considered: erythrocytes having numerous, fine, uniform spicules throughout the cell membrane (echinocytes) and erythrocytes irregularly shaped without defined spicules (Figure 3a and b). Erythrocytes with these distorted shapes can be commonly observed in blood analysis since they are often overlooked as an artifact of preparation (i.e. effects of glass and blood storage). The echinocytic transformation is caused by significant alterations in the RBC membrane with expansion of the outer leaflet and compression of the inner and it is favoured by intercalation of amphiphilic molecules into the out layer of the RCB plasma membrane bilayer [37, 38]. The exogeneously induced discocyte-echinocyte transformation is generally reversible, indicating that this RBC shape transformation is usually not connected to some irreversible change in the conformation of the membrane skeleton or the membrane bilayer [39]. However, the peculiarity of echinocytes to be rigid and nondeformable may reduce the blood flow in the microcirculation or cause microvascular injury processes [38–40]. Therefore, the quantification of the echinocyte formation can have diagnostic application.

The scattering properties of echinocytes gave rise to four spectral signatures (Figure 3d–g), two found also for ordinary RBCs (Endmembers 2 and 3) and two new ones (Endmembers 5 and 6). The latters are characterized by a significant blue-shift of the component at lower wavelength (from ~510 to ~460 and ~480 nm, respectively) and a relevant red-shift of the band at higher wavelength (from ~590 to ~660 and 640 nm, respectively). These spectral shifts could be indicative of changes in protein compositions connected to morphological alterations. On one hand many proteins possess multi-wavelength UV-visible fingerprints which shifts when the environment conditions changes. For example, erythrocytes contain a significant physiological concentration of haemoglobin, which exhibits some characteristic bands (i.e. at about 550 and 580 nm) which shift when hemolysis occurs or depending on haemoblobin oxygenation state [41]. From the other hand, it is known that some factors causing echinocytic transformation affect RBC endogenous proteins, inducing transformation and rearrangement or aggregation of proteins (i.e. an

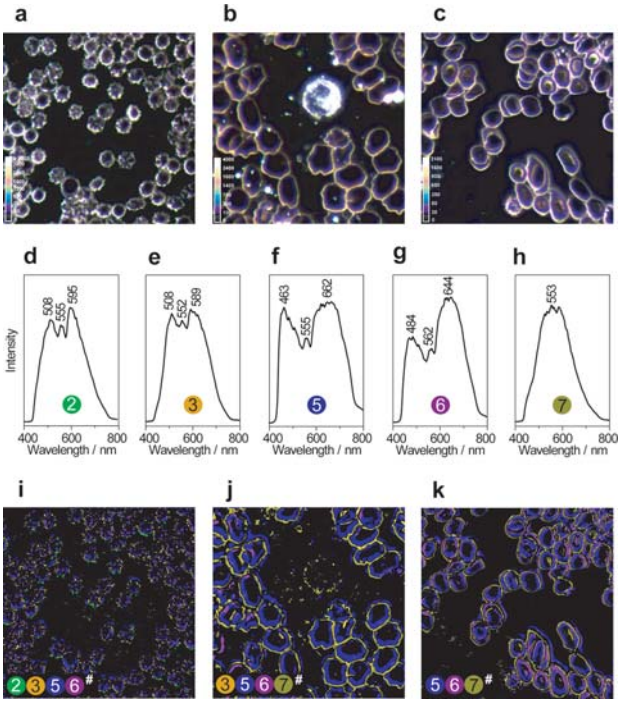

Figure 3 RBCs with deformed morphology. (**a**) Hyperspectral images of Echynocytes, (**b**) Irregularly shaped RBCs, and (**c**) RBCs from a blood sample of an individual suffering of non-allergetic food intolerance; (**d**–**h**) Spectral libraries and (**i**–**k**) Hyperspectral images showing the location of each endmembers in the image scenes. (#) Colored circles indicating the spectral signatures found by SAM analysis in the hyperspectral images. Images were acquired by using 100× objective. The intensity values are color-coded according to the color scale bar All images are 60 μm × 60 μm.

increase in intracellular Ca(II) concentration of RBCs, as well as ATP depletion) [19, 37, 42].

The effectiveness of the identified spectral libraries was verified by the spectral mapping (Figure 3i), evidencing a quite similar contribution from all the endmembers (∼25%) (Figure 4a).

As regards irregularly shaped RBCs, the EDFM image showed also in this case that the light scattering properties of these RBCs are affected by the morphological changes (Figure 3b). In fact, the image analysis revealed the presence of four distinct endmembers, three of them just found for ordinary RBCs (Endmember 3) and echynocytes (Endmembers 5 and 6), respectively (Figure 3e–h). The new spectral pattern (Endmember 7), which is different from the others, is characterized by the presence of only one broad band centered at ∼550 nm. By using these endmember spectra, a satisfactory mapping analysis of samples was obtained, as shown in Figure 3j.

The effectiveness of the identified spectral libraries was tested in the SAM analysis of hyperspectral images from blood samples of individuals having non-allergic food hypersensitivity. The EDFM images showed RBCs not uniform in shape and having circles inside (Figure 3c), thus quite different from ordinary RBCs appearing as round circles (Figure 1a). In the literature this appearance has been interpreted as indication of nutritionally deficiency of cells [43]. The image spectra of these RBCs were compared with all the seven spectral libraries found for the ordinary and deformed RBCs, and only three spectral patters (Endmembers 5–7) were found in the scanned area of the samples (Figure 3k). Since these three spectral signatures are peculiar for RBCs with membrane alterations (echynocytes and RBCs irregularly shaped, respectively) and none for healthy RBCs, the no-ordinary condition of the individuals was confirmed (Figure 4c).

Local cell membrane curvature determined by the orientation of blood cells relative to the propagation vector of the illuminating electro-magnetic field could have a significant influence. However, the analysis of different samples where RBCs were randomly-oriented and the good matches constantly achieved by

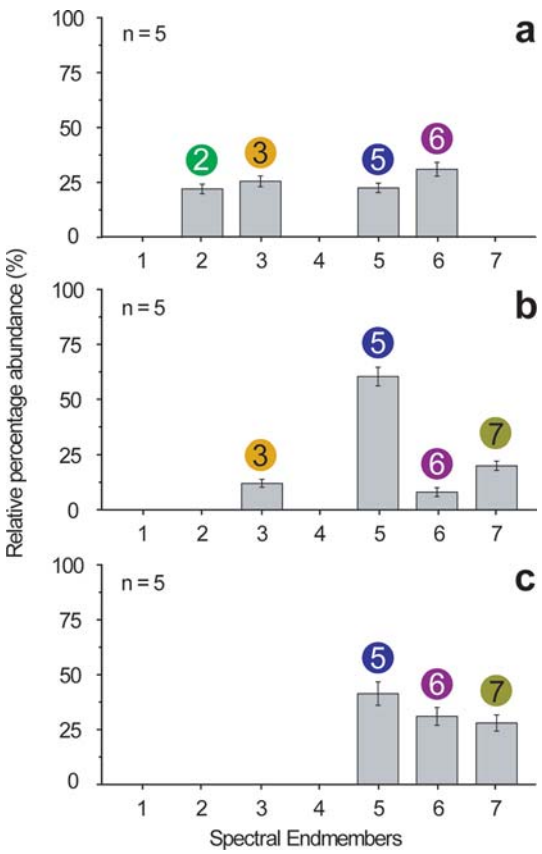

Figure 4 Relative percentage abundance of the spectral libraries, revealed by the SAM analysis of the hyperspectral images of (**a**) Echynocytes, (**b**) Irregularly shaped RBCs, and (**e**) RBCs of some individuals suffering of non-allergetic food intolerance. *n* standing for the number of the analysed samples.

the mapping of the build-up libraries with a small spectral angle (0.1 in radians) onto images taken from them, let us to conclude that the spectral signatures identified are not sensitively affected by the cell orientation, but probably result from a particular curvature of the membrane surface connected with the morphological state. Thus, they are peculiar of the different morphological alterations analysed.

In conclusion, the existence of different scattering spectra associable to morphologic alterations in RBCs can be a key step for a rapid and early detection of a potential unhealthy state of individuals.

3.2 White Blood cells (WBCs)

The hyperspectral imagery technique was also tested on neutrophil granulocytes, the most abundant type of WBCs in mammals. Granulocytes play a crucial role in the first-line defense against invading bacteria, fungi and protozoa. The neutrophils-mediated inflammatory response can be regarded as a multi-step process whose most of steps are dependent on the mobilization of cytoplasmic granules and secretory vesicles.

The EDFM measurements were performed on neuthrophils during all the stages of their life-cycle for testing if it is possible to differentiate active from inactive WBCs by spectral signatures. Under normal condition, non-activated neuthrophils have a quite spheric shape (see Figure 1), whose the image derived endmembers resulted to be two, one characterized by a broad band having two main peaks at ~520 and ~600 nm, and another one having a less symmetric shape and a maximum at ~620 nm (Figure 5a and b). These two spectral endmembers were used in the SAM mapping analysis of RBC hyperspectral images to verify the inactivity of granulocytes if present (white area in Figures 1c and 2c).

When neuthrophils are activated they start to swell and, once the swelling reaches the breakage critical limit of cell membrane, they break up with the subsequent leakage of the internal granules. As expected, also the spectral patterns of granulocytes are affected by activation (Figure 5c), but the image analysis revealed the presence of only one endmember during all the stages of the activated WBC life-cycle. In fact, a good match across all the hyperspectral images of activated granulocytes was obtained by using this endmember (Figure S4 in Supplementary Information). This finding is in agreement with the literature reporting that the early phases of the changes in light-scattering properties of human neutrophils after stimulation are not a consequence of neutrophil degranulation, but membrane ruffling, affecting the polarization of the neutrophil morphology [44–46].

In conclusion, the hyperspectral microscopic analysis of neutrophils showed to be able to detect the distinct functional state of neutrophils (active and inactive) on the basis of distinct spectral libraries. This properties may be of help in yielding information on the extent of prior cell activation.

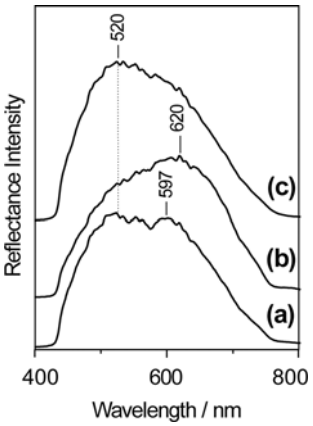

Figure 5 Spectral libraries of netrophil granulocytes. (**a**–**b**) VNIR spectra of inactive and (**c**) active neutrophils obtained by using hyperspectral imager. The spectrum intensity has been normalized.

4. Conclusion

Biomedical technologies including new drug development, cell cloning and regeneration, biotherapeutics, and so on, need to visualize live cell and cellular mechanism. Hyperspectral Imaging System (HIS) integrated on a microscopy is a technique not yet widely spread that can be very useful in biological sample analysis, since it allows both the observation of live cells without an invasive sample preparation and the use of light scattering properties of cells.

The hyperspectral image acquisition and analysis of the two main components present in human blood, RBCs and WBCs, showed to be effective in giving qualitative and quantitative data on the transformation of these blood cells. Thanks to the property of HIS to detect changes in light scattering properties of these blood components, it was possible characterize specific spectral signatures of the ordinary state of both RBCs and WBCs, as well as build-up spectral libraries associable both to deformed RBCs and WBCs in an activated state.

This is a preliminary, yet important contribution, to the application of the Darkfield microscopy based hyperspectral analysis to blood cell screening for clinical use. These results motivate further studies to evaluate significant correlations of RBC and WBC spectral features in healthy conditions and in patients affected by specific pathologies, especially for coupling with molecular information obtained from membrane proteomics and lipidomics [29–32].

Acknowledgements The authors thank PM.06.006 of CNR (Italy), Drs. Sam Lawrence and Jamie Uertz (CytoViva Inc., Auburn AL) for technical support. A.G.L gratefully acknowledges CSIC (Spain) for JAE-Pre 2011 Grant.

Author biographies Please see Supporting Information online.

References

[1] B. S. Sorg, B. J. Moeller, O. Donovan, Y. Cao, and M. W. Dewhirst, J Biomed Opt. **10**, 44004/1-44004/11 (2005).
[2] M. E. Martin, M. B. Wabuyele, K. Chen, P. Kasili, M. Panjehpour, M. Phan, B. Overholt, G. Cunningham, D. Wilson, R. C. Denovo, and T. Vo-Dinh, Ann. Biomed. Eng. **34**, 1061–1068 (2006).
[3] S. J. Leavesley, N. Annamdevula, J. Boni, S. Stocker, K. Grant, B. Troyanovsky, T. C. Rich, and D. F. Alvarez, J. Biophotonics **5**, 67–84 (2012).
[4] T. A. Harris, Cytometry Part A, **69A**, 872–879 (2006).
[5] A. R. Badireddy, M. R. Wiesner, and J. Liu, Environ. Sci. Technol. **46**, 10081–10088 (2012).
[6] R. A. Schultz, T. Nielsen, J. R. Zavaleta, R. Ruch, R. Wyatt, and H. R. Garner, Cytometry **43**, 239–247 (2001).
[7] A. Rocha, Y. Zhou, S. Kundu, J. M. González, S. Bradleigh Vinson, and H. Liang, J. Nanobiotechnology **9**, 1–9 (2011).
[8] V. Vodyanoy, Micros. Today **13**, 26–28 (2005).
[9] J. Beach, BioOptics World, **3** (2009).
[10] H. Grahn and P. Geladi, in: Techniques and Applications of Hyperspectral Image Analysis (John Wiley and Sons Ltd., Chichester, West Sussex, 2009), p. 361.
[11] M. Diez-Silva, M. Dao, J. Han, and S. Suresh, MRS Bull. **35**, 382–388 (2010).
[12] J. P. Mills, L. Qie, M. Dao, C. T. Lim, and S. Suresh, Mech Chem Biosyst. **1**, 169–80 (2004).
[13] A. Chabanel, M. Flamm, K. L. Sung, M. M. Lee, D. Schachter, and S. Chien, Biophys J. **44**, 171–176 (1983).
[14] G. Popescu, Y. K. Park, W. Choi, R. R. Dasari, M. S. Feld, and K. Badizadegan, Blood Cells Mol Dis. **41**, 10–16 (2008).
[15] M. Kinnunen, A. Kauppila, A. Karmenyan, and R. Myllyla, Biomed. Opt. Express. **2**, 1803–1814 (2011).
[16] Ö. Ergül, A Arslan-Ergül, and L. Gürel, J. Biomed. Opt. **15**, 045004/1–045004/8 (2010).
[17] J. He, A. Karlsson, J. Swartling, and S. Andersson-Engels, J. Opt. Soc. Am. A **21**, 1953–1961 (2004).
[18] Y. Park, C. A. Best-Popescu, R. R. Dasari, and G. Popescu, J. Biomed. Opt. **16**, 011013/1–011013/7 (2011).
[19] M. P. Sheetz, and S. J. Singer, J. Cell Biol. **73**, 638–646 (1977).
[20] Y. K. Park, M. Diez-Silva, D. Fu, G. Popescu, W. Choi, I. Barman, S. Suresh, and M. S. Feld, J. Biomed. Opt. **15**, 020506/1–020506/3 (2010).
[21] Y. K. Park, M. Diez-Silva, G. Popescu, G. Lykotrafitis, W. Choi, M. S. Feld, and S. Suresh. Proc. Natl. Acad. Sci. USA, **105**, 13730–13735 (2008).
[22] B. K. Wilson, M. R. Behrend, M. P. Horning, and M. C. Hegg, Opt. Express **19** (2011).
[23] D. Tycko, M. Metz, E. Epstein, and A. Grinbaum, Appl. Opt. **24**, 1355–1365 (1985).
[24] J. M. Steinke and A. P. Shepherd, Appl. Opt. **27**, 4027–4033 (1998).
[25] R. A. Meyer, Appl Opt. **16**, 2036–2037 (1977).
[26] N. K. Uzunoglu, D. Yova, and G. S. Stamatakos, J. Biomed. Opt. **2**, 310–318 (1997).
[27] S. V. Tsinopoulos, J. E. Sellountos, and D. Polyzos, Appl. Opt. **41**, 1408–1417 (2002).
[28] A. Vainrub, O. Pustovyy, and V. Vodyanoy, Opt. Lett. **31**, 2855–2857 (2006).
[29] E. M. Pasini, H. U. Lutz, M. Mann, and A. W. Thomas, J Proteom. **73**, 421–435 (2010).
[30] J. G. Mohanty, H. D. Shukla, J. D. Williamson, L. J. Launer, S. Saxena, and J. M. Rifkind, Proteome Sci. **8**, 11 (2010).
[31] C. Ferreri, F. Angelini, C. Chatgilialoglu, S. Dellonte, V. Moschese, P. Rossi, and L. Chini, Lipids **40**, 661–667 (2005).
[32] A. A. Puca, P. Andrew, V. Novelli, C. V. Anselmi, F. Somalvico, N. A. Cirillo, C. Chatgilialoglu, and C. Ferreri, Rejuvenation Res. **11**, 63–72 (2008).
[33] B. J. Bain In: S. M. Lewis, B. J. Bain, and I. Bates (eds.), Dacie and Lewis practical haematology. 10th ed. (Churchill Livingston Elsevier, Philadelphia 2006), pp. 80–113.
[34] A. L. Copley, Clin. Hemorheol. **7**, 3–14 (1987).
[35] N. Abramson, Blood **107**, 4205 (2006).
[36] C. Le Devehat, M. Vimeux, and A. Bertrand, J. Mal, Vasc. **14**, 307–311 (1989).
[37] B. Agroyannis, A. Dalamangas, H. Tzanatos, C. Fourtounas, I. Kopelias, I. Konstadinidou, and D. Koutsikos, Blood **84**, 1685–1686 (1994).
[38] A. Iglic, V. Kralj-Iglic, and H. Hagerstrand, Eur. Biophys. J. **27**, 335–339 (1998).
[39] G. Brecher and M. Bessis, Blood **40**, 333–344 (1972).
[40] B. E. Glader and J. L. Lukens In: Lee G. R., Foerster J., Lukens J., Paraskevas F., Greer J. P., Rodgers G. M. (eds.), Wintrobe's Clinical Hematology, Hereditary spherocytosis and other anemias due to abnormalities of the red cell membrane, 10th ed., Vol. 1 (Williams & Wilkins, Baltimore, Lippincott, 1998), pp. 1132–1159.
[41] A. Nonoyama, In: Using multiwavelength UV-visible spectroscopy for the characterization of red blood cells: An investigation of hypochromism. Graduate School Theses and Dissertations (2004), http://scholarcommons.usf.edu/etd/1179.
[42] B. Jones, T. F. Walker, S. B. Chahwala, M. C. Thompson, and J. A. Hickman, Exp Cell Res **168**, 309–317 (1987).
[43] M. L. Turgeon, Clinical Hematology: Theory and Procedures. 4th ed., Vol. 936 (Williams & Wilkins, Baltimore, Lippincott, 2004), pp. 99–111.
[44] P. L. McNeil, A. L. Kennedy, A. S. Waggoner, D. L. Taylor, and R. F. Murphy, Cytometry **6**, 7–12 (1985).
[45] M. P. Fletcher and B. E. Seligmann, J. Leukoc. Biol. **37**, 431–447 (1985).
[46] D. Y. Orlova, M. A. Yurkin, A. G. Hoekstra, and V. P. Maltsev, J. Biomed. Opt. **13**, 054057/1–054057/7 (2008).

